International Clinical Case Reports and Reviews
2025 Volume 3, Issue 2
DOI: 10.59657/2993-0855.brs.25.029

BioRes Scientia
Value your Research

Review Article

Open Access

Magnetic Resonance Imaging of the Lumbar Spine: The most Effective Diagnostic Method for Assessing Lower Back Pain

Ajay Deep Singh, Dilshad Ahmad*

Department of Radio Imaging Technology, Era University, Lucknow, India.

**Corresponding author: Dilshad Ahmad.*

Abstract

Low back pain (LBP) is a prevalent and debilitating condition that affects approximately 9.6% of the global population, making it one of the leading causes of healthcare consultations. It is the primary contributor to years lived with disability and ranks third in terms of health expenditure, following diabetes and ischemic heart disease. The management of LBP is often complicated by the unnecessary use of imaging, particularly in patients without red flags. The Choosing Wisely campaign highlights the need to reduce excessive imaging and interventions, which increase healthcare costs. Magnetic resonance imaging (MRI) is the preferred diagnostic tool when conservative treatments fail, especially in patients with concerning clinical signs, such as those with a history of spinal surgery, older adults, and individuals with conditions like osteoporosis or malignancies. Unlike radiography and computed tomography (CT), MRI offers superior tissue contrast resolution and avoids ionizing radiation. A thorough understanding of spinal anatomy, especially the structure of the cervical, thoracic, and lumbar regions, is essential in assessing degenerative changes and their implications for low back pain. This paper reviews the significance of MRI in evaluating low back pain, its role in clinical decision-making, and the anatomical foundations necessary for accurate interpretation.

Keywords: low back pain (LBP); MRI (magnetic resonance imaging); healthcare expenditure; spine anatomy; degenerative changes; conservative management; imaging guidelines; choosing wisely campaign; disability-adjusted life years (DALY); clinical decision-making; spinal disorders; spinal cord; vertebral anatomy

Introduction

Low back pain is a prevalent condition that significantly affects both patient health and healthcare expenditures. Approximately 9.6% of the global population is impacted, making it one of the primary reasons individuals consult primary healthcare providers. It is noteworthy that nearly everyone will encounter lower back pain at some stage in their lives [1,2]. Low back pain ranks as the leading cause of years lived with disability and is the third most significant contributor to disability-adjusted life years [3]. The third most demanding condition of health expenditure is low back and neck pain, after diabetes and ischaemic heart disease [4]. The Choosing Wisely campaign is focusing on the imaging of patients who do not present red flags, as this practice is often excessive. Conducting investigations and surgical procedures for patients experiencing low back pain before attempting conservative management significantly increases healthcare costs. [5,6]. 1. In cases where conservative treatment for low back pain is ineffective, magnetic resonance imaging (MRI) is the preferred method for additional assessment. Imaging is particularly important for patients exhibiting concerning clinical signs, especially those with a history of surgery, older adults, individuals on long-term steroid therapy, or those with osteoporosis, low-impact injuries, suspected or confirmed malignancies, infections, or immunosuppressed conditions. MRI provides enhanced tissue contrast resolution compared to radiography and computed tomography (CT), which are less effective in evaluating the spinal cord and involve exposure to ionizing radiation [7].

Spine anatomy

The spinal column consists of seven cervical, twelve thoracic, five lumbar, five sacral, and four coccygeal vertebrae. Understanding the anatomical and physiological differences among these spinal regions is crucial for identifying common sites of degenerative changes and for the assessment of these areas through MRI. The development of the spine and spinal cord is intricately linked, despite originating from distinct progenitor cells. Each vertebra comprises a vertebral body and the posterior elements, also known as the neural arch. The intervertebral discs separate the vertebral bodies of the cervical, thoracic, and lumbar

regions, contributing to both stability and the transfer and distribution of weight. The neural arch encases and safeguards the spinal cord.

Most vertebrae originate from three primary ossification centres, with the notable exception of the second cervical vertebra. Primary ossification commences in utero during the first trimester and is typically completed by the end of the first year. Secondary ossification centres include the endplate annular apophyses and the apophyses of the transverse and spinous processes, with variability observed in the secondary ossification centres of the first and second cervical vertebrae. This secondary ossification process begins at puberty and generally concludes by the third decade of life.

The first cervical vertebra, known as the atlas, and the second cervical vertebra, referred to as the axis, exhibit specialized anatomical and functional characteristics. The atlas features an anterior and posterior arch along with lateral masses that articulate with the head and axis, respectively. Its elongated transverse processes extend laterally from the lateral masses. The axis is distinguished by the odontoid process, or dens, which is a superior extension of the body that enables rotation in conjunction with the atlas. The body of the axis is robustly supported laterally to facilitate articulation with the lateral masses of the atlas above and the superior articular processes of C3 below.

Like all remaining vertebrae, the axis has posterior elements that are composed of (short) pedicles, (thick) laminae, and a (long) spinous process.

The remainder of the cervical vertebrae, C3 to C7, the thoracic vertebrae, and the lumbar vertebrae are composed of vertebral bodies and the posterior elements or neural arch. The first components of the neural arch extending posterolateral from the vertebral body are the pedicles. Extending laterally from the pedicles are the transverse processes. More posteriorly, the spinal canal is shielded by the laminae, where they meet at the midline origin of the spinous processes. Therefore, the osseous spinal canal is formed by the posterior margin of the vertebral body, bilateral pedicles, and bilateral laminae (fig 1).

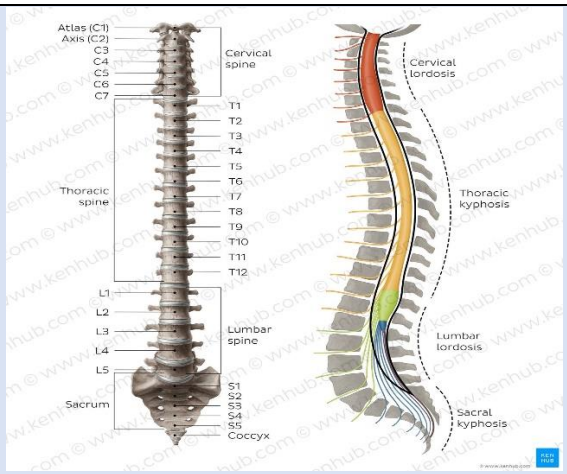

Figure 1: Spine Anatomy (image copyright www.kenhub.com)

The intervertebral or neural foramina convey the nerve roots for each spinal nerve at each level. These are bounded by the inferolateral corner of the posterior vertebral body and the intervertebral disc anteriorly (as well as by the uncinate processes in the cervical spine), by pedicles both superiorly and inferiorly, and by the facet joint (as well as by the articular pillar of the cervical spine) posteriorly. The zygapophyseal or facet joints, between superior and inferior articular processes on adjacent vertebra, are predominantly oriented in the coronal plane, except in the lumbar spine where they are oriented in an oblique sagittal plane.

The spinal column consists of seven cervical, twelve thoracic, five lumbar, five sacral, and four coccygeal vertebrae. Understanding the anatomical and physiological differences among these spinal regions is crucial for identifying common sites of degenerative changes and for the assessment of these areas through MRI. The development of the spine and spinal cord is intricately linked, despite originating from distinct progenitor cells. Each vertebra comprises a vertebral body and the posterior elements, also known as the neural arch. The intervertebral discs separate the vertebral bodies of the cervical, thoracic, and lumbar regions, contributing to both stability and the transfer

and distribution of weight. The neural arch encases and safeguards the spinal cord.

Most vertebrae originate from three primary ossification centers, with the notable exception of the second cervical vertebra. Primary ossification commences in utero during the first trimester and is typically completed by the end of the first year. Secondary ossification centers include the endplate annular apophyses and the apophyses of the transverse and spinous processes, with variability observed in the secondary ossification centers of the first and second cervical vertebrae. This secondary ossification process begins at puberty and generally concludes by the third decade of life.

The first cervical vertebra, known as the atlas, and the second cervical vertebra, referred to as the axis, exhibit specialized anatomical and functional characteristics. The atlas features an anterior and posterior arch along with lateral masses that articulate with the head and axis, respectively. Its elongated transverse processes extend laterally from the lateral masses. The axis is distinguished by the odontoid process, or dens, which is a superior extension of the body that enables rotation in conjunction with the atlas. The body of the axis is robustly supported laterally to facilitate articulation with the lateral masses of the atlas above and the superior articular processes of C3 below.

The C3 to C7 vertebrae uniquely possess uncinate processes, which are hook-shaped superior extensions located at the posterolateral edges of the vertebral bodies. The transverse processes of the cervical vertebrae feature transverse foramina that accommodate the passage of the vertebral arteries, which typically enter at the C6 level. Additionally, the cervical spine contains articular pillars, which are bony structures situated just behind the transverse processes and adjacent to the pedicle-lamina junctions, providing support to the superior and inferior articular processes. Unlike the spinous processes of the thoracic and lumbar regions, the cervical vertebrae exhibit bifid spinous processes. Furthermore, the spinous processes of both the cervical and thoracic vertebrae are longer and exhibit a more inferior angulation compared to those of the lumbar vertebrae.

The thoracic vertebrae connect with their corresponding ribs at two distinct points. The rib origins engage with shallow facets located at the posterosuperior and posteroinferior edges of the thoracic vertebrae. Additionally, the rib tubercles, which are small projections located just distal to the rib heads, articulate with small articular facets found on the transverse processes of the thoracic vertebrae. In contrast, the lumbar vertebral bodies and transverse processes are the largest and longest, respectively. The lumbar articular processes, which extend both superiorly and inferiorly from the pedicle-lamina junction, create a structure known as the pars interarticularis. The laminae of the lumbar spine also provide posterior protection to the spinal canal, although they do not overlap to the same extent as the laminae in the cervical and thoracic regions.

The stabilization of the spine is primarily facilitated by the ligaments and paraspinal muscles. The craniocervical junction, characterized by its complexity, comprises several stabilizing ligaments. Among the ligaments specific to this junction are the anterior atlanto-occipital membrane (AAOM), apical ligament, alar ligaments, cruciate ligament, and the posterior atlanto-occipital membrane (PAOM) (Figure 2).

The AAOM spans from the anterior edge of the clivus to the anterior arch of the atlas, continuing downward as the anterior atlanto-axial membrane (AAAM) from the anterior arch of the atlas to the anterior edge of the axis, and subsequently as the anterior longitudinal ligament (ALL). Although the apical ligament, which runs from the tip of the clivus (basion) to the tip of the dens, is notable, it does not contribute significantly to stabilization. The alar ligaments originate from the lateral curved edges at the tip of the dens and attach to the medial edges of both occipital condyles. Positioned just behind the dens, the cruciate ligament features both horizontal and vertical components. The more robust horizontal bands extend laterally, connecting to tubercles at the medial edges of the atlas, while the vertical bands run craniocaudally, linking to the posterior edges of the clivus and dens, respectively. The PAOM stretches from the posterior lip of the foramen magnum (opisthion) to the posterior arch of the atlas, followed by the posterior atlantoaxial membrane (PAAM), which connects the posterior arch of the atlas to the laminae of the axis.

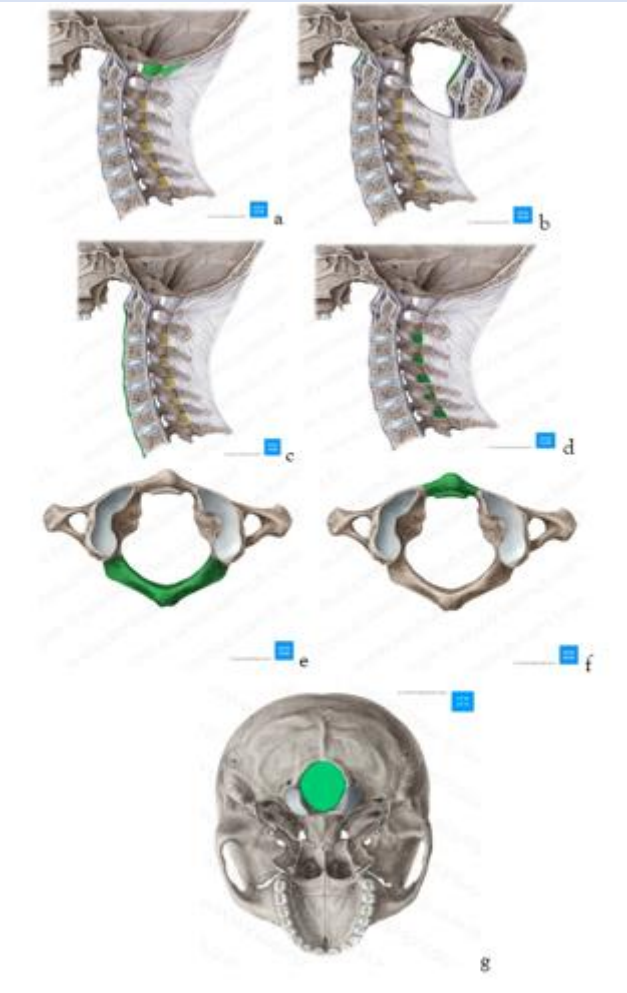

Figure 2: a] Posterior atlantooccipital membrane, b] Anterior atlantooccipital membrane, c] Anterior longitudinal ligament, d] Ligamenta flava, e], Posterior arch of atlas, f] Anterior arch of atlas, g] Foramen magnum

The posterior longitudinal ligament (PLL) is situated along the back edge of the vertebral bodies. At its superior end, it attaches to the posterior aspect of the axis body, subsequently broadening to form the tectorial membrane. This membrane continues upward, merging with the dura mater at the posterior edge of the clivus. The PLL exhibits a broader and more secure attachment to the intervertebral discs compared to the vertebral bodies, which contrasts with the anterior longitudinal ligament (ALL), that is more firmly anchored to the vertebral bodies than to the intervertebral discs. The ALL is positioned along the front edge of the vertebral bodies and extends superiorly at the level of the axis body as the anterior atlanto-axial membrane (AAAM) and subsequently as the anterior atlanto-occipital membrane (AAOM). Inferiorly, both the ALL and PLL taper at their respective connections to the anterior and posterior edges of the sacral body. The ligamenta flava are analogous to the anterior atlanto-axial and anterior atlanto-occipital membranes, as they connect the laminae of adjacent vertebrae from C2-C3 to L5-S1. Additionally, the spinous processes are linked by ligaments known as interspinous ligaments. The supraspinous ligament spans the tips of adjacent spinous processes from C7 to S1. Above C7, this ligament transitions into the significantly thicker nuchal ligament, which also attaches to the remaining cervical spinous processes and the posterior tubercle of the atlas, ultimately connecting to the inion or the midline of the external occipital protuberance. The spinal cord represents the caudal extension of the medulla oblongata, beginning below the foramen magnum and descending through the spinal canal until it concludes at the conus medullaris, typically at the L1 level in adults. A slender fibrous strand known as the filum terminale extends downward from the apex of the conus medullaris, anchoring into the first coccygeal segment. The nerve roots that extend downward from the conus medullaris are collectively referred to as the cauda equina.

The human spinal column comprises eight cervical, twelve thoracic, five lumbar, five sacral, and one coccygeal paired nerve roots. The cervical nerve roots

emerge from the neural (or intervertebral) foramen that aligns with the more caudal segment at the level of the intervertebral disc (for instance, the C5 nerve root exits via the C4-C5 neural foramen). An exception to this pattern is observed with the C8 nerve roots, which exit through the C7-T1 neural foramen. In contrast, the thoracic, lumbar, and S1 to S4 nerve roots exit through the neural foramen corresponding to the more cranial segment at the intervertebral disc level (for example, the L4 nerve roots exit through the L4-L5 neural foramen). The S5 and coccygeal nerve roots exit through the sacral hiatus.

Transitional lumbosacral vertebra

Accurate labeling of vertebral levels and the recognition of the transitional lumbosacral vertebra (TLV) are essential for precise reporting and for preventing spinal procedures from being conducted at incorrect levels. TLVs are hybrid vertebrae located at the interface between the lumbar spine and the sacrum. These vertebrae are relatively prevalent, with an overall occurrence rate of 18.1%, and they are found more frequently in males (28.1%) compared to females (11.1%) [8]. The phenomenon of lumbarisation of the S1 vertebral body is less common than the sacralisation of L5 [9]. Identifying the L5 nerve root, which is unique as the only lumbar nerve root lacking proximal branching, can facilitate the accurate labeling of the L5 vertebra, even in cases of sacralisation, achieving an accuracy rate of 98% [10]. The iliolumbar ligament is identified in 85.7% of cases and extends from the transverse process of L5 to the iliac wing in 96% of instances, serving as a significant anatomical landmark for the identification of vertebral levels [11]. While these techniques are effective in accurately determining the L5 vertebra, it is essential to communicate the existence of transitional lumbar vertebrae (TLV) and to document the methodology used for lumbosacral segment labeling to referring clinicians. This practice is crucial in order to avert the risk of performing surgical procedures at incorrect vertebral levels. The most precise approach for labeling vertebral segments involves total spine imaging, which can be achieved by referencing previous studies or by obtaining comprehensive spine radiographs.

Intervertebral disc anatomy

Intervertebral discs are fibrocartilaginous entities situated between two neighbouring vertebral bodies. These discs function as fibrocartilaginous joints, permitting a limited range of bending movements in various directions, including flexion, extension, lateral flexion, and torsion. Additionally, they act as ligaments that stabilize the spine and serve as shock absorbers to reduce axial loading on the spinal column. Anatomically, each disc consists of an outer annulus fibrosus and an inner nucleus pulposus, which are connected to the cartilaginous endplates of the adjacent vertebrae. The annulus fibrosus is made up of multiple lamellated layers of collagen, providing a robust circumferential exterior that encases the nucleus pulposus and attaches to the vertebral endplates, thereby offering tensile and radial strength. The nucleus pulposus, characterized by its gelatinous composition of loose collagen, proteoglycans, and water, functions as a shock absorber, imparting compressive strength to the disc. It is important to note that the intervertebral disc is avascular, obtaining nutrients from capillaries located within the vertebral endplates and depending on passive diffusion to nourish the disc cells.

Disc degeneration

On MRI, a healthy intervertebral disc exhibits a clear distinction between the nucleus pulposus and the annulus fibrosus, characterized by a high T2-weighted signal intensity in the nucleus pulposus and a comparatively lower T2-weighted signal intensity in the surrounding annulus fibrosus, reflecting the differences in water content (Figure 5). Disc degeneration encompasses a variety of pathophysiological changes that lead to a decline in the functionality of the intervertebral disc. Factors influencing disc degeneration include mechanical stress, aging, lifestyle choices (such as smoking), and genetic factors [12]. The impact of these elements results in a reduction of hydrophilic proteoglycans and, consequently, water content in the nucleus pulposus, which diminishes its ability to withstand axial loading. In addition to disc desiccation, disc degeneration involves numerous degenerative processes affecting both the intervertebral disc and the adjacent vertebral endplates, including narrowing of the disc space, fibrosis, the vacuum disc phenomenon, annular fissures, erosion of endplate cartilage, marginal osteophyte formation, and Modic changes in the endplate.

The MRI characteristics of disc degeneration are most effectively identified using T2-weighted sequences. These characteristics include a reduction in T2-weighted signal within the intervertebral disc, a loss of the normal distinction between the nucleus pulposus

and annulus fibrosus, and ultimately a decrease in the height of the intervertebral disc. A grading system for the morphological alterations of the intervertebral disc on T2-weighted sequences was developed by Pfirrmann et al. and subsequently revised by Griffith et al., primarily to ensure standardization across various research studies [13,14].

Annular fissures are commonly observed in cases of disc degeneration and are defined as disruptions in the fibers of the annulus fibrosus, occurring either within its structure or at its junction with the vertebral body. On MRI, annular fissures are indicated by linear hyperintensity on T2-weighted images and may show contrast enhancement within the disc due to the presence of fluid and the infiltration of vascularized granulation tissue (fig 3).

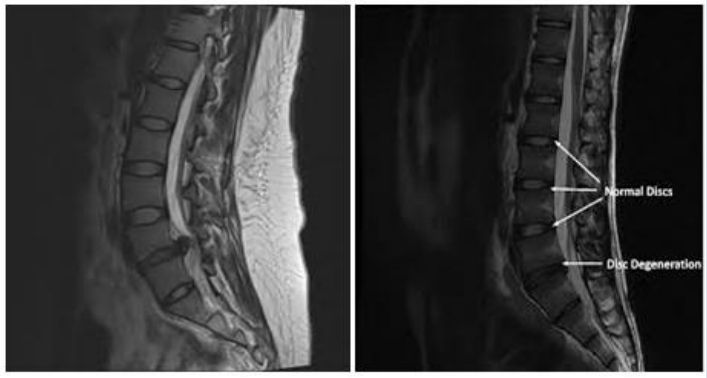

Figure 3: Disc Degeneration

Disc bulge and disc herniation

In 2014, a revision of the recommendations concerning lumbar disc nomenclature was issued by collaborative task forces from the North American Spine Society, the American Society of Spine Radiology, and the American Society of Neuroradiology. These revised guidelines aim to standardize the terminology used in radiological reports regarding lumbar disc degeneration, reflecting the advancements in understanding that have emerged in the medical literature since the initial recommendations were published in 2001. The definitions of disc bulge, disc herniation, and their respective locations are derived from these 2014 nomenclature guidelines. Disc bulge is defined as a broad-based protrusion of the disc that extends beyond the edges of the adjacent vertebral endplates. For a protrusion to be classified as a disc bulge, it must exceed 90° of the disc's circumference beyond the vertebral endplate margins. When a disc bulge extends posteriorly into the spinal canal, it may project symmetrically into both the right and left sides of the canal, or it may be asymmetric, favoring one side over the other. Notably, disc bulges consist solely of the annulus fibrosus. Conversely, disc herniation is characterized by a more localized extension of the disc, affecting less than 90° of the intervertebral disc's circumference beyond its normal boundaries. This condition arises from a rupture in the annulus fibrosus, which permits the nucleus pulposus to protrude into the resulting defect. Unlike disc bulges, herniations are more likely to elicit symptoms, as they typically extend further from the original disc and may come into contact with and irritate the spinal cord or nerve roots.

Disc herniations can be categorized based on their morphology into two main types: disc protrusions and disc extrusions. A disc protrusion is characterized by a broad base, where the width of the base exceeds that of any other segment of the herniation (refer to Figure 11). In contrast, a disc extrusion features a base that is narrower than the herniation itself in any given plane (see Figure 4). This narrow attachment of the disc extrusion to its originating disc may facilitate upward or downward movement of the herniation within the spinal canal, known as cranial or caudal migration, respectively. Should the connection between a disc extrusion and its originating disc be severed, it results in disc sequestration. Consequently, disc sequestration leads to a free fragment of the intervertebral disc residing within the spinal canal, detached from its original disc. Such sequestrations may also exhibit cranial or caudal migration within the spinal canal. It is essential for radiologists to identify and accurately describe the positioning of these free intervertebral disc fragments, as they may remain unnoticed during surgical procedures.

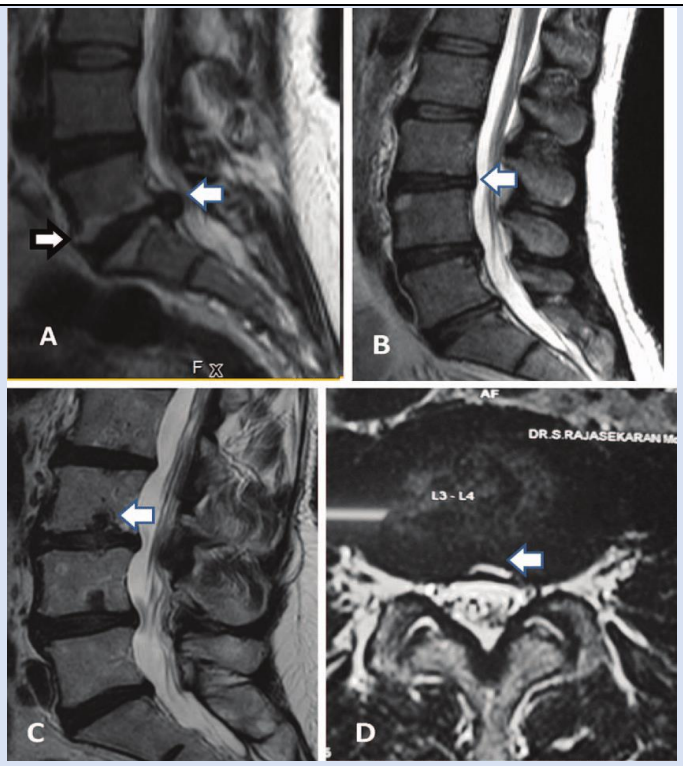

Figure 4: MRI phenotypes. (A) Disc bulge and herniations (white arrow) were diagnosed when the annulus was bulged beyond the posterior vertebral border of the disc in sagittal T2 MRI images. Modic changes were assessed in the sagittal sequences based on standard end plate signal changes (white arrow with black outline). (B) Pfirrmann grading was scored on the basis of signal changes (white arrow) in the discs in T2 sagittal images. (C) Schmorl node was documented in sagittal T2 MRI images as focal endplate defects (white arrow). (D) Annular tears/ high-intensity zones were defined as focal areas of high signal intensity on axial T2 images near the posterior disc annulus (white arrow) (uploaded by Senthil Natesan).

Spine location reporting

The location of a lumbar disc herniation is key in determining which cauda equina nerve root(s) may be affected. Lesions in the spinal canal can be classified as central, subarticular, foraminal, or extraforaminal, based on their position relative to the intervertebral disc (see Figure 14A) [18]. Central herniations occur medially within the spinal canal, between the medial edges of the facet joints, and can be midline or slightly off-center (right or left). They may cause spinal canal stenosis and a posterior mass effect on the cauda equina nerve roots but rarely compress a single nerve root. The subarticular zone, located laterally in front of the facet joint, contains transiting cauda equina nerve roots that exit through the lower neural foramen. Subarticular herniations can compress these nerve roots, leading to radiculopathy at the level below the herniation (e.g., an L3-L4 subarticular herniation can affect the L4 nerve root). Further lateral is the foraminal zone, where disc herniations extend into the lumbar neural foramina, located beneath the pedicle and in front of the inferior articular pillar.

The extraforaminal zone is located laterally to the foraminal zone, where disc herniations extend outside the pedicle and may compress nearby nerves, causing radiculopathy similar to foraminal herniations (e.g., an L3-L4 extraforaminal herniation can lead to L3 radiculopathy). Lesions in the spinal canal can be classified by their position relative to the intervertebral disc and pedicle into discal, infrapedicular, pedicular, or suprapedicular zones. This classification, along with length measurements, helps delineate the craniocaudal position and extent of disc extrusions or sequestrations, best illustrated through sagittal imaging.

Facet and uncovertebral joint arthrosis

The facet joints, or zygapophyseal joints, are paired synovial joints between neighboring vertebrae that facilitate movement while restricting excessive flexion, extension, anterior translation, and rotation. The uncovertebral joints, or Luschka joints, are also paired synovial joints located at the posterolateral edges of intervertebral discs in the lower cervical spine (C2-C3 to C6-C7). They guide cervical spine flexion and extension, limit lateral flexion, and help prevent disc herniation.

Both facet and uncovertebral joints can undergo degenerative changes due to mechanical stress and

aging, often alongside disc degeneration. Facet arthrosis can be detected on MRI through indicators like joint space narrowing, irregular articular surfaces, subarticular erosions, osteophyte formation, and facet hypertrophy. These changes can reduce the size of the adjacent neural foramen. Normal synovial fluid in facet joints is usually not visible on MRI, while facet joint effusions appear as increased T2-weighted hyperintense fluid [19,20].

Synovial cyst

Synovial cysts are defined as encapsulated protrusions of synovial fluid that arise from degenerated facet joints and extend beyond the joint space. These cysts are predominantly found in the lumbar spine, although they can develop at any facet joint. When these cysts extend anteriorly from the facet joint into the spinal canal, they may lead to subarticular recess or spinal canal stenosis. In the lumbar region, synovial cysts that occupy the subarticular recess can compress the transiting cauda equina nerve roots, which exit at the next most caudal neural foramen (for instance, an L4-L5 synovial cyst may compress the L5 nerve root within the L4-L5 subarticular recess). On MRI, synovial cysts typically appear hyperintense on T2-weighted images, with a hypointense rim adjacent to the facet joint located in the posterolateral aspects of the spinal canal. In cases of previous hemorrhage, the contents of the cyst may exhibit varying T1-weighted and T2-weighted signal characteristics. The presence of signal void and susceptibility within the cyst, indicative of gas, is characteristic of a synovial cyst, as it signifies a connection with the vacuum joint phenomenon of the neighboring facet joint. Post-gadolinium T1-weighted imaging reveals that synovial cysts may show varying degrees of peripheral enhancement and are frequently associated with additional findings such as facet arthrosis and joint effusion (fig 5).

Figure 5: Synovial cyst

Spinal canal, subarticular recess, and neural foraminal narrowing

In addition to its role in providing mechanical support for maintaining an upright posture and facilitating flexible movement, the spine serves to protect the spinal cord and nerve roots. The spinal canal, which is the cavity located within the vertebral column, houses the spinal cord, conus medullaris, and cauda equina nerve roots. The configuration of the spinal canal varies due to the anatomical differences among the cervical, thoracic, and lumbar vertebrae; nevertheless, the overall boundaries of the spinal canal remain relatively consistent throughout the spine. The anterior boundary is formed by the posterior aspects of the vertebral bodies, intervertebral discs, and the posterior longitudinal ligament, while the posterior boundary consists of the facet joints, laminae, and ligamentum flavum. The paired neural foramina on either side facilitate the passage of exiting nerve roots at each intervertebral level. Degenerative changes in the spine can encroach upon the spinal canal or neural foramina, potentially leading to damage of the spinal cord or nerve roots. Various methods exist for quantifying spinal canal stenosis and spinal cord compression through the assessment of canal dimensions, cross-sectional area, and dimensional ratios. Although many of these techniques are time-intensive and may not be practical for clinical use, advancements in computer automation may enhance their applicability in the future. The average sagittal diameter of the cervical spinal canal observed on MRI is approximately 13.7-14.1 mm. A sagittal diameter of less than 13 mm is regarded as relatively narrowed, while a measurement below 10 mm is classified as absolutely narrowed, based on cervical spine radiographs correlated with

myelopathy symptoms. MRI offers the advantage of detecting contributions from soft tissue structures that may narrow the thecal sac, such as disc herniations and thickening of the ligamentum flavum.

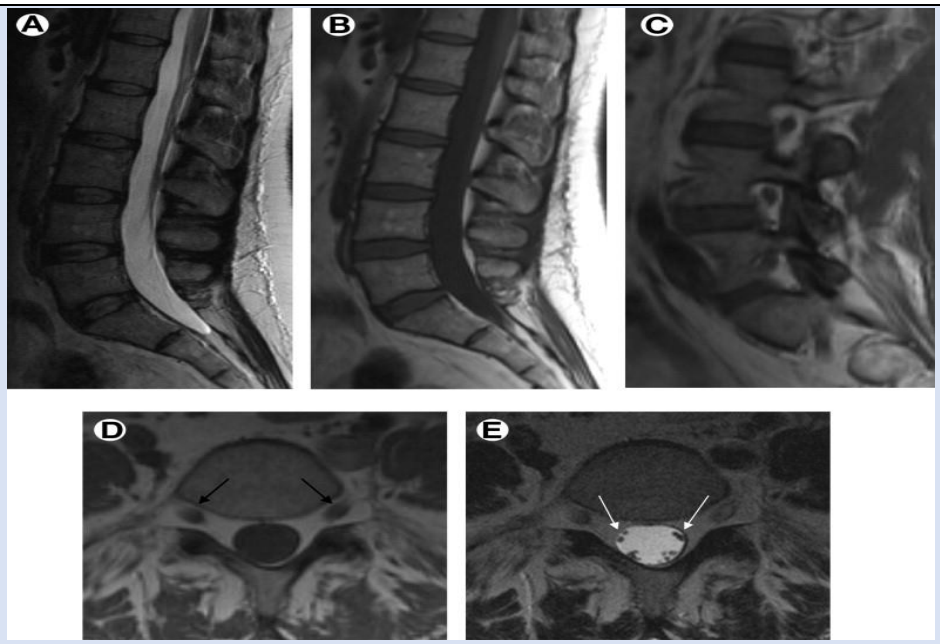

Figure 6

Spondylolysis and spondylolisthesis

Spondylolysis, characterized by defects in the pars interarticularis, represents stress fractures typically found in the lower lumbar region of the spine. While many individuals may not exhibit symptoms, these defects can lead to localized pain, especially during physical activity or spinal extension. Magnetic resonance imaging (MRI) can reveal osseous defects in the pars interarticularis, along with bone marrow edema and/or an increased sagittal dimension of the spinal canal due to the distraction of the posterior elements (refer to Figure 20A) [21]. Furthermore, spondylolysis may result in spinal malalignment, where the affected vertebra is positioned anteriorly in relation to the adjacent caudal vertebra, a condition known as isthmic spondylolisthesis. These abnormalities are most effectively visualized using sagittal imaging sequences. The literature indicates that the diagnostic accuracy of MRI for spondylolysis varies significantly, ranging from 36% to 97% [44,45]. This discrepancy is likely due to multiple factors. In comparison to computed tomography (CT), MRI is less adept at identifying abnormalities in cortical bone, which can lead to false-negative results. Conversely, false-positive results may arise from the thinning of the pars interarticularis, osseous sclerosis, or the partial volume averaging of adjacent marginal osteophytes associated with facet arthrosis [22]. Bone scintigraphy, particularly when combined with single photon emission computed tomography (SPECT) and CT, is recognized as the most sensitive method for detecting symptomatic spondylolysis. The CT component of this examination identifies osseous defects in the pars interarticularis, while SPECT highlights the physiological changes associated with increased bone turnover at the site of the stress fracture [23].

Figure 7

Baastrup syndrome and intraspinal posterior epidural cyst

Baastrup syndrome, commonly referred to as kissing spine syndrome, is a painful disorder characterized by the contact between neighboring spinous processes in the lumbar region, leading to the formation of pseudo-articulations and degenerative alterations. This condition manifests as localized midline pain that is alleviated by flexion and worsened by extension. Magnetic resonance imaging (MRI) findings indicative of Baastrup syndrome include hypertrophy of the lumbar spinous processes, contact between these processes, T2 hyperintense fluid accumulation in the bursa situated between the spinous processes, irregularities and sclerosis of the affected bony cortex, as well as bone marrow edema beneath the pseudo-articulations (Figure 21) [50]. A possible complication associated with Baastrup syndrome is the emergence of an intraspinal posterior epidural cyst. This cyst represents an anterior extension of bursal formation between the lumbar spinous processes, which exerts a mass effect on the posterior epidural space, potentially leading to varying degrees of spinal canal stenosis [24]. In contrast to synovial cysts that extend from adjacent facet joints into the posterolateral region of the spinal canal, intraspinal posterior epidural cysts protrude into the midline of the posterior epidural space.

Spine infection

Acute pyogenic spondylodiscitis

Understanding the MRI characteristics of acute pyogenic spondylodiscitis, also known as discitis-osteomyelitis, necessitates a comprehension of the underlying pathophysiology associated with this infectious condition. The intervertebral discs lack a direct blood supply and depend on the abundant end arteries located within the metaphyseal regions beneath the vertebral endplates for their nutrient acquisition. These end arteries serve as the primary sites for the haematogenous seeding of bacteria originating from septic microthrombi during episodes of bacteraemia. Following the onset of vertebral endplate osteomyelitis, the proteolytic enzymes secreted by bacteria facilitate the contiguous spread of infection into the adjacent intervertebral disc and ultimately to the contralateral vertebral endplate, leading to the development of both discitis and osteomyelitis [25].

The initial MRI findings indicative of acute pyogenic spondylodiscitis include alterations in bone marrow signal and the destruction of a singular vertebral endplate. On T1-weighted (T1W) and T2-weighted (T2W) imaging, the cortex of the vertebral endplate is visualized as a thin dark margin. In cases of osteomyelitis, the absence of this dark margin signifies cortical destruction. Inflammation of the bone marrow manifests as T1W hypointensity, with the marrow exhibiting a signal intensity lower than that of adjacent muscle on T1W images, alongside T2W hyperintensity and post-gadolinium enhancement. Additional early MRI findings may include inflammatory enhancement and T2W hyperintensity within the paravertebral soft tissues or the epidural space. As the infection advances, MRI findings will reveal both discitis and osteomyelitis affecting the intervertebral disc and the adjacent vertebral endplates. The presence of concomitant discitis is characterized by T2W hyperintensity, resembling water signal intensity, accompanied by post-gadolinium enhancement. As proteolytic enzymes degrade the intervertebral disc, a reduction in disc

height is observed. The imaging features with the highest sensitivity for diagnosing pyogenic spondylodiscitis include the presence of paraspinal or epidural inflammation [26].

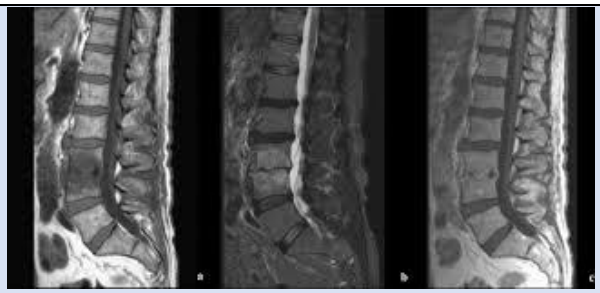

Figure 8

Epidural abscess

Spinal epidural abscess represents a critical infection within the epidural space, leading to the accumulation of pus that can cause mechanical compression or vascular impairment of the spinal cord or cauda equina. This infection is predominantly pyogenic, with Staphylococcus aureus being the most common causative agent, followed by coagulase-negative staphylococci (such as S. epidermidis), Escherichia coli, and Pseudomonas aeruginosa. Additionally, it may arise from mycobacterial, fungal, or parasitic origins. The development of spinal epidural abscesses can occur through direct inoculation during recent surgical procedures or spinal interventions, contiguous spread from associated discitis-osteomyelitis, or through haematogenous dissemination [27].

Magnetic resonance imaging (MRI) is the most reliable imaging technique for identifying spinal epidural phlegmon and abscess. Epidural phlegmon is characterized by a mass-like collection of inflammatory tissue in the epidural space that lacks identifiable drainable pus. On MRI, this condition is noted for its homogeneous or slightly heterogeneous enhancement and T2-weighted hyperintense material within the epidural area. In contrast, an epidural abscess is identified as a peripherally enhancing T2 hyperintense fluid collection within the epidural space. The non-enhancing purulent material will also exhibit restricted diffusion on diffusion-weighted imaging. It is crucial to assess the length of the abscess, the pattern of enhancement, the extent of spinal canal stenosis, the mass effect on the thecal sac and spinal cord, and the presence or absence of spinal cord edema, as these parameters can aid in prognostic evaluation. MRI findings may also reveal underlying discitis-osteomyelitis or septic facet arthritis [28].

Figure 9

Septic facet arthritis

The facet or zygapophysial joints of the spine are bilateral synovial joints located between the articular processes of adjacent vertebrae, playing a crucial role in guiding and restricting spinal movement. Septic facet arthritis arises from bacterial or fungal infections of the facet joint, which may occur due to direct inoculation, such as during therapeutic facet joint injections, or through hematogenous dissemination. Typically, septic facet arthritis presents unilaterally; however, there are instances where the infection may extend to the contralateral facet joint via the retrodural space of Okada [31].

Imaging findings associated with septic facet arthritis often overlap with those of active synovitis linked to degenerative facet arthrosis. These findings include joint effusions, enhancement of the synovial lining, erosions of the articular surface, subchondral marrow edema, and periarticular inflammation. Consequently, correlating these imaging results with the patient's medical history, clinical assessment, and serum inflammatory markers is essential for suggesting a diagnosis of septic facet arthritis. The presence of restricted diffusion in facet effusions would indicate the presence of purulent material within the joint space, characteristic of septic facet arthritis. Additionally, adjacent posterior epidural inflammatory changes, epidural abscesses, or paraspinal abscesses are indicative of septic facet arthritis rather than facet arthrosis [32].

Insufficiency and Pathologic Fractures

Stress fractures occur when there is a disparity between the mechanical load applied and the strength of the bone structure. Fatigue fractures, a specific type of stress fracture, arise when the bone's architecture is intact, yet the mechanical load is heightened due to increased repetition, duration, or intensity. The resulting microtrauma cannot be adequately repaired or remodeled before additional microtrauma occurs, leading to the development of fatigue fractures. Insufficiency fractures, another variant of stress fractures, occur when the mechanical load is normal, but the underlying bone structure is compromised, either due to imbalances in bone remodelling processes or other factors [33].

Conclusions

Back and neck pain are ubiquitous in today's society, a common cause of disability, and a large burden to healthcare costs. When conservative management of low back or neck pain fails, MRI is the imaging modality of choice to assess for underlying abnormality. Knowledge of spine anatomy and imaging features of degenerative changes allow for appropriate reporting and directs appropriate patient management. MRI is also useful in detecting non-degenerative spine conditions, such as infection or insufficiency fractures, which may have a similar clinical presentation.

Conflict of interest

The authors report no conflict of interest.

References

1. Hoy D, March L, Brooks P, et al. (2014). The global burden of low back pain: estimates from the global burden of disease 2010 study. *Ann Rheum Dis*, 73:968-974.
2. Maher C, Underwood M, Buchbinder R. (2017). Non-specific low back pain. *Lancet*, 389:736-747.
3. Murray CJ, Lopez AD. (2013). Measuring the global burden of disease. *N Engl J Med*, 369:448-457.
4. Dieleman JL, Baral R, Birger M, et al. (2016). US spending on personal health care and public health, 1996-2013. *JAMA*, 316:2627-2646.
5. Rao VM, Levin DC. (2012). The overuse of diagnostic imaging and the Choosing Wisely initiative. *Ann Intern Med*, 157:574-576.
6. Kim LH, Vail D, Azad TD, et al. (2019). Expenditures and health care utilization among adults with newly diagnosed low back and lower extremity pain. *JAMA Netw Open*, 2:e193676.
7. Patel ND, Broderick DF, Burns J, et al. (2016). ACR appropriateness criteria: lower back pain. *Journal of the American College of Radiology*, 13(9):1069-1078.
8. Nardo L, Alizai H, Virayavanich W, et al. (2012). Lumbosacral transitional vertebrae: association with low back pain. *Radiology*, 265:497-503.
9. Konin GP, Walz DM. (2010). Lumbosacral transitional vertebrae: classification, imaging findings, and clinical relevance. *AJNR Am J Neuroradiol*, 31:1778-1786.
10. Peckham ME, Hutchins TA, Stilwill SE, et al. (2017). Localizing the L5 vertebra using nerve morphology on MRI: an accurate and reliable technique. *AJNR Am J Neuroradiol*, 38:2008-2014.
11. Carrino JA, Campbell PD Jr, Lin DC, et al. (2011). Effect of spinal segment variants on

numbering vertebral levels at lumbar MR imaging. *Radiology*, 259:196-202.
12. Choi YS. (2009). Pathophysiology of degenerative disc disease. *Asian Spine J*, 3:39-44.
13. Pfirrmann CW, Metzdorf A, Zanetti M, et al. (2001). Magnetic resonance classification of lumbar intervertebral disc degeneration. *Spine*, 26:1873-1878.
14. Griffith JF, Wang YX, Antonio GE, et al. (2007). Modified Pfirrmann grading system for lumbar intervertebral disc degeneration. *Spine*, 32:E708-712.
15. Modic MT, Steinberg PM, Ross JS, et al. (1988). Degenerative disk disease: assessment of changes in vertebral body marrow with MR imaging. *Radiology*, 166:193-199.
16. Jenson RK, Leboeuf-Yde C, Wedderkopp N, et al. (2012). Is the development of modic changes associated with clinical symptoms? A 14-month cohort study wih MRI. *Eur Spine J*, 21:2271-2279.
17. Crockett MT, Kelly BS, van Baarsel S, et al. (2017). Modic type 1 vertebral endplate changes: injury, inflammation, or infection? *AJR Am J Roentgenol*, 209:167-170.
18. Wiltse LL, Berger PE, McCulloch JA. (1997). A system for reporting the size and location of lesions in the spine. *Spine*, 22:1534-1537.
19. Hartman J. (2014). Anatomy and clinical significance of the uncinate process and uncovertebral joint: a comprehensive review. *Clin Anat*, 27:431-440.
20. Weishaupt D, Zanetti M, Boos N, et al. (1999). MR imaging and CT in osteoarthritis of the lumbar facet joints. *Skeletal Radiol*, 28:215-219.
21. Ulmer JL, Mathews VP, Elster AD, et al. (1997). MR imaging of lumbar spondylolysis: the importance of ancillary observations. *AJR Am J Roentgenol*, 169:233-239.
22. Yamaguchi KT Jr, Skaggs DL, Acevedo DC, et al. (2012). Spondylolysis is frequently missed by MRI in adolescents with back pain. *J Child Orthop*, 6:237-240.
23. Ganiyusufoglu AK, Onat L, Karatoprak O, et al. (2010). Diagnostic accuracy of magnetic resonance imaging versus computed tomography in stress fractures of the lumbar spine. *Clin Radiol*, 65:902-907.
24. Johnson DW, Farnum GN, Latchaw RE, et al. (1989). MR imaging of the pars interarticularis. *AJR Am J Roentgenol*, 152:327-332.
25. Trout AT, Sharp SE, Anton CG, et al. (2015). Spondylolysis and beyond: value of SPECT/CT in evaluation of low back pain in children and young adults. *Radiographics*, 35:819-834.
26. Filippiadis DK, Mazioti A, Argentos S, et al. (2015). Baastrup's disease (kissing spines syndrome): a pictorial review. *Insights Imaging*, 6:123-128.
27. Chen CK, Yeh L, Resnick D, et al. (2004). Intraspinal posterior epidural cysts associated with Baastrup's disease: report of 10 patients. *AJR Am J Roentgenol*, 182:191-194.
28. Ratcliffe JF. (1985). Anatomic basis for the pathogenesis and radiologic features of vertebral osteomyelitis and its differentiation from childhood discitis. A microarteriographic investigation. *Acta Radiol Diagn*, 26:137-143.
29. Ledermann HP, Schweitzer ME, Morrison WB, et al. (2003). MR imaging findings in spinal infections: rules or myths? *Radiology*, 228:506-514.
30. Moritani T, Kim J, Capizzano AA, et al. (2014). Pyogenic and non-pyogenic spinal infections: emphasis on diffusion-weighted imaging for the detection of abscesses and pus collections. *Br J Radiol*, 87:20140011.
31. Patel KB, Poplawski MM, Pawha PS, et al. (2014). Diffusion-weighted MRI claw sign improves differentiation of infectious from degenerative modic type 1 signal changes of the spine. *AJNR Am J Neuroradiol*, 35:1647-1652.

Cite this article: Singh A D, Ahmad D. (2025). Magnetic Resonance Imaging of the Lumbar Spine: The most Effective Diagnostic Method for Assessing Lower Back Pain, *International Clinical Case Reports and Reviews*, BioRes Scientia Publishers. 3(2):1-13. DOI: 10.59657/2993-0855.brs.25.029

Article History: **Received:** February 10, 2025 | **Accepted:** February 28, 2025 | **Published:** March 05, 2025